

S-matrix poles near the Thresholds in the Coupled $\Lambda N - \Sigma N$ System

K. Miyagawa and H. Yamamura

Department of Applied Physics, Okayama University of Science

1-1 Ridai-cho, Okayama 700, Japan

(February 5, 2020)

Abstract

We search t -matrix poles for the $\Lambda N - \Sigma N$ coupling interaction. The two soft core models of the Nijmegen group which bind the hypertriton at the correct binding energy and the hard core models which are still influential on hypernuclear physics are investigated. A useful method of calculating the off-shell t -matrix of a hard core potential is proposed. We find poles close to the ΣN threshold in the second or third quadrant of the complex plane of the ΣN relative momentum. The relation between the nearby poles and the shape of the ΛN elastic total cross section is discussed based on a so-called uniformization by which two-channel t -matrices become single-valued on a complex variable. We find also poles near the ΛN threshold. Those are correlated to the S -wave ΛN scattering lengths the values of which have not yet been determined.

13.75.Ev, 21.45.+v, 21.30.-x, 21.80+a

I. INTRODUCTION

Recent theoretical analyses of few-baryon systems with strangeness such as the three-body calculations of $^3\Lambda H$ [1–3] and the four-body study of $^4\Lambda H$ [4] have promising new features. Most of our knowledge of the underlying YN interaction has been obtained from heavier hypernuclei and it remains rather qualitative. In contrast, those few-body analyses are based on modern baryon-baryon forces and on rigorous solutions of the few-body Schrödinger equations, thus they have the great advantage to scrutinize YN interaction models. As an example references [1–3] demonstrated that the Nijmegen soft core YN interaction [5] binds the hypertriton, but the Jülich \tilde{A} potential [6] does not. This is possibly caused by the sizable difference between the 1S_0 force components showing up in the low-energy region [2]. This points to the fact that even basic quantities such as scattering lengths are not yet well determined, and modern meson-theoretical interactions suffer from that.

Another interesting result in these few-body analyses is the effect of the $\Lambda - \Sigma$ conversion which was exactly included in a coupled channel formalism [1]. Although in the case of the hypertriton the admixture of ΣNN states is only 0.5%, the expectation values of the sum of the transition potentials $V_{\Lambda N, \Sigma N}$ and $V_{\Sigma N, \Lambda N}$ turned out to be about 8% of the total potential energy, which is crucial for the binding of the hypertriton [2,3].

This knowledge about the coupling to the Σ states, however, is obtained from the bound state lying below the ΛNN threshold. This should be extended to analyses close to the Σ threshold, where $\Lambda - \Sigma$ conversion effects will emerge sharply. Experimentally in this region so-called unstable bound states [7] have received attention and have been searched for various hypernuclei. Only one state in the $\Sigma(\Lambda)NNN$ system is confirmed in the reaction $^4He(K^-, \pi^-)$ [8]. The existence of such an unstable bound state in the $A=4$ system was predicted by Harada *et al.* where the coupling to continuum ΛNNN states was approximated by a ΣN optical potential [9]. However, for understanding real features of $\Lambda - \Sigma$ conversion, it is highly desirable to treat it directly using a realistic $\Lambda N - \Sigma N$ coupling interaction.

At present, only for the ΣN and ΣNN systems it is technically possible to incorporate precisely the coupling to Λ continuum states. Afnan and Gibson [10] calculated the Λd elastic scattering fully incorporating this coupling but using simple phenomenological YN interactions. They found and analyzed enhancements just below the ΣNN threshold. We are interested not only in a similar study applying more sophisticated meson-theoretical interactions, but also in the analysis of other isospin states, which will be experimentally accessible through electromagnetic hyperon-production processes [11]. Thereby it will become possible to really examine the $\Lambda N - \Sigma N$ coupling interaction.

Let us turn to the YN interaction. There exists a variety of strengths for the $\Lambda N - \Sigma N$ coupling among extensively used meson-theoretical potentials. The soft core model [5] and the hard core model D [12] of the Nijmegen group show cusps in the ΛN elastic total cross section just at the ΣN threshold with different magnitudes, while the Nijmegen hard core model F [13] and the Jülich models [6] show round resonance peaks below the threshold. We stress here that these prominent cusps do not mean simple threshold effects, but suggest the existence of t -matrix poles in unphysical Riemann sheets. This point of view is important because these poles might move and become unstable bound state poles if the coupling strengths varied. Some examples for separable potentials are given in Ref. [15], and we shall locate these poles and follow their trajectories in this paper for the Nijmegen potentials.

One of the authors (K.M.) prepares the analysis of $\Lambda NN - \Sigma NN$ continuum states using meson-theoretical interactions, to which the knowledge of YN t -matrix around the ΣN threshold is crucial. This paper accordingly investigates poles of the t -matrices for the Nijmegen F, D and the two soft core interactions [5,14]. This is done in momentum space and hence the results are directly applicable to the three-body calculation. The behavior of t -matrices around an inelastic threshold in coupled channel problems and the effects of nearby poles have often been studied (see Ref. [16], and the references are therein). In such analyses the key points are to understand the connection of various Riemann energy sheets and how far from the physical region the poles are located. We adopt in this analysis a so-called uniformization given by Newton [17], by which the t -matrix for two-channel problems becomes single-valued after a suitable variable is introduced in place of energy. We thereby clearly describe the positions and the trajectories of the t -matrix poles in the Riemann sheets.

Section II gives the expression for $\Lambda N - \Sigma N$ t -matrix which is analytically continued to the complex energy plane. Section III describes a way to treat a hard core potential in momentum space. This is done for the purpose of treating the Nijmegen hard core potentials which are influential even now. In Sec. IV, the uniformization mentioned above is introduced, thereby we discuss how the shape of the ΛN elastic total cross section around the ΣN threshold is related to the positions of nearby poles. In Sec. V, the positions of the t -matrix poles for the Nijmegen soft and hard core models are displayed. We also show the trajectories of the poles when the strengths of the potentials are increased. Section VI summarizes and concludes the paper.

II. ANALYTIC CONTINUATION OF THE T -MATRIX

In this section we give the expression of the off-shell t -matrix for the $\Lambda N - \Sigma N$ system and analytically continue it into the complex energy plane.

The coupled t -matrices for the $\Lambda N - \Sigma N$ system are defined by the integral equations

$$T_{ij}(z) = V_{ij} + \sum_k V_{ik} G_0^{(k)}(z) T_{kj}(z), \quad i, j, k = 1, 2 \quad (2.1)$$

with

$$G_0^{(k)}(z) = (z - H_0^{(k)})^{-1}, \quad z = E + i\varepsilon \quad (2.2)$$

where the numbers 1 and 2 are assigned to the ΛN and ΣN channels, respectively. The free Hamiltonian $H_0^{(k)}$ for channel k is defined as

$$H_0^{(k)} = \frac{p_k^2}{2\mu_k} + m_N + m_Y^{(k)} \quad (2.3)$$

This refers to the total momentum zero frame and we denote the relative momentum between

the nucleon and the hyperon by \mathbf{p}_k and the reduced mass of channel k by μ_k . The masses $m_Y^{(k)}$ ($k = 1, 2$) indicate m_Λ and m_Σ respectively. After the partial-wave decomposition in momentum space, we express the projected T -matrix elements for a given total angular momentum and a parity again simply by T . Then Eq. (2.1) reads

$$\begin{aligned} < p | T_{ij}(z) | p' > &= < p | V_{ij} | p' > \\ &+ \sum_k \int_0^\infty dp'' p''^2 < p | V_{ik} | p'' > \frac{1}{e_k - \frac{p''^2}{2\mu_k} + i\varepsilon} < p'' | T_{kj}(z) | p' > \end{aligned} \quad (2.4)$$

with

$$e_k \equiv \frac{q_k^2}{2\mu_k} = E - m_N - m_Y^{(k)} . \quad (2.5)$$

For the sake of a simple notation we dropped the index on p and we assumed that the partial-wave elements have no coupling between different orbital angular momenta nor between channel-spin states. The extension to the case with the couplings is straightforward.

Let us now consider the energy E , and hence e_k as well as

$$q_k = \sqrt{2\mu_k e_k} \quad (2.6)$$

to be complex numbers. We introduce the function

$$h_k(p'') \equiv < p | V_{ik} | p'' > < p'' | T_{kj}(z) | p' > \quad (2.7)$$

and define each term in the k -summation of the right-hand side of Eq. (2.4) by $I_k(e_k)$:

$$I_k(e_k) = \int_0^\infty dp'' \frac{p''^2 h_k(p'')}{e_k - \frac{p''^2}{2\mu_k}} . \quad (2.8)$$

This function has a cut for $e_k \geq 0$ or, expressed in terms of E , a cut along $m_N + m_Y^{(k)} \leq E < \infty$. There are thus two cuts in the E plane starting at the $N + \Lambda$ and $N + \Sigma$ thresholds, respectively. The function values beyond the cuts are defined by analytic continuation. To do this we modify this equation as

$$I_k(e_k) = \int_0^\infty dp'' \frac{p''^2 h_k(p'') - 2\mu_k e_k h_k(q_k)}{e_k - \frac{p''^2}{2\mu_k}} + h_k(q_k) \int_0^\infty dp'' \frac{2\mu_k e_k}{e_k - \frac{p''^2}{2\mu_k}} \quad (2.9)$$

where we assume that $h_k(p)$ can be continued analytically and has no singularity moving

from real p to the complex value q_k given in Eq. (2.6). This is true in our case. We see that now the cut appears explicitly in the the second term of Eq. (2.9). One easily finds

$$\int_0^\infty dp'' \frac{2\mu_k e_k}{e_k - \frac{p''^2}{2\mu_k}} = -i\pi\mu_k \sqrt{2\mu_k e_k} = -i\pi\mu_k q_k \quad (2.10)$$

which defines the integral in both sheets of the Riemann e_k surface corresponding to positive and negative imaginary parts of q_k . According to Eqs. (2.9) and (2.10), we rewrite Eq. (2.4) as

$$\begin{aligned} & \langle p | T_{ij}(z) | p' \rangle = \langle p | V_{ij} | p' \rangle \\ & + \sum_k \left[\int_0^\infty dp'' \left(\frac{p''^2 \langle p | V_{ik} | p'' \rangle \langle p'' | T_{kj}(z) | p' \rangle}{e_k - \frac{p''^2}{2\mu_k}} \right. \right. \\ & \left. \left. - \frac{2\mu_k e_k \langle p | V_{ik} | q_k \rangle \langle q_k | T_{kj}(z) | p' \rangle}{e_k - \frac{p''^2}{2\mu_k}} \right) - i\pi \mu_k q_k \langle p | V_{ik} | q_k \rangle \langle q_k | T_{kj}(z) | p' \rangle \right]. \end{aligned} \quad (2.11)$$

We recognize that this equation contains a new t -matrix element $\langle q_k | T_{kj} | p' \rangle$ which requires the additional equation

$$\begin{aligned} & \langle q_k | T_{ij}(z) | p' \rangle = \langle q_k | V_{ij} | p' \rangle \\ & + \sum_k \left[\int_0^\infty dp'' \left(\frac{p''^2 \langle q_k | V_{ik} | p'' \rangle \langle p'' | T_{kj}(z) | p' \rangle}{e_k - \frac{p''^2}{2\mu_k}} \right. \right. \\ & \left. \left. - \frac{2\mu_k e_k \langle q_k | V_{ik} | q_k \rangle \langle q_k | T_{kj}(z) | p' \rangle}{e_k - \frac{p''^2}{2\mu_k}} \right) - i\pi \mu_k q_k \langle q_k | V_{ik} | q_k \rangle \langle q_k | T_{kj}(z) | p' \rangle \right]. \end{aligned} \quad (2.12)$$

These Eqs. (2.11) and (2.12) form a closed set of integral equations [18] and define the t -matrix elements on the entire q_k planes or the Riemann surface of the complex energy E . This is the set we solved.

III. T -MATRIX FOR A HARD CORE POTENTIAL

Although it has become old-fashioned to represent the short-range repulsion of the NN interaction by a hard core, the Nijmegen D and F models of the YN interaction with hard cores are still used in hypernuclear physics. We therefore explore a method to obtain the off-shell t -matrix for a hard core potential in momentum space, which is shown in this section.

The off-shell t -matrix can be expressed as

$$\langle \vec{p} | T(z) | \vec{k} \rangle = \langle \vec{p} | V | \Psi_{q, \vec{k}}^{(+)} \rangle \quad (3.1)$$

where $\Psi_{q, \vec{k}}^{(+)}$ is defined by

$$| \Psi_{q, \vec{k}}^{(+)} \rangle = | \vec{k} \rangle + G_0(z) V | \Psi_{q, \vec{k}}^{(+)} \rangle \quad (3.2)$$

with

$$z = \frac{q^2}{2\mu} + i\varepsilon \quad . \quad (3.3)$$

We omit the $\Lambda N - \Sigma N$ coupling for the sake of a simple notation. Let us first divide the interaction V into the pure hard core part U and the remainder \hat{V} as

$$V = U + \hat{V} \quad (3.4)$$

and use the two-potential formula [19]

$$\langle \vec{p} | T(z) | \vec{k} \rangle = \langle \vec{p} | U | \Phi_{q, \vec{k}}^{(+)} \rangle + \langle \Phi_{q, \vec{p}}^{(-)} | \hat{V} | \Psi_{q, \vec{k}}^{(+)} \rangle \quad (3.5)$$

with

$$| \Phi_{q, \vec{k}}^{(+)} \rangle = | \vec{k} \rangle + G_0(z) U | \Phi_{q, \vec{k}}^{(+)} \rangle \quad , \quad (3.6)$$

$$| \Phi_{q, \vec{p}}^{(-)} \rangle = | \vec{p} \rangle + G_0(z^*) U | \Phi_{q, \vec{p}}^{(-)} \rangle \quad . \quad (3.7)$$

As we shall show later, the first term of the right-hand side of Eq. (3.5) is expressed analytically, and the second term satisfies an integral equation similar to the Lippmann-Schwinger equation which can be solved in an ordinary way. Our method is thus a natural extension of a usual treatment without a hard core, and is useful not only for the present purpose, but also for other few-body calculations in momentum space.

The analytic expression of the first term in Eq. (3.5) was already given by Takemiya [20], who proposed a method to evaluate the off-shell t -matrix for a hard-core potential in coordinate space. We only use this method to treat the pure hard-core part in the formula (3.5). Let us expand the Φ 's in Eqs. (3.6) and (3.7) into partial waves

$$\Phi_{q, \vec{k}}^{(\pm)}(\vec{r}) = \sum_{\substack{l's' \\ ls \\ JM}} y_{l's'}^{JM}(\hat{r}) \Phi_{l's'ls}^{J(\pm)}(q, k, r) y_{ls}^{JM\dagger}(\hat{k}) \quad (3.8)$$

and similarly Ψ . Here, y_{LS}^{JM} is the simultaneous eigenfunction of L^2 , S^2 , J^2 and J_z . We denote the pure-hard core part of Eq. (3.5) as

$$\langle \vec{p} | \tilde{t}(z) | \vec{k} \rangle \equiv \langle \vec{p} | U | \Phi_{q, \vec{k}}^{(+)} \rangle \quad (3.9)$$

and also decompose it into partial waves

$$\langle \vec{p} | \tilde{t}(z) | \vec{k} \rangle = \sum_{\substack{l's' \\ ls \\ JM}} y_{l's'}^{JM}(\hat{r}) \tilde{t}_{l's'ls}^J(p, k; z) y_{ls}^{JM\dagger}(\hat{k}) . \quad (3.10)$$

Reference [20] proves that if we introduce a function χ defined by

$$\frac{\chi_{l's'ls}^{J(\pm)}(q, k, r)}{r} \sqrt{\frac{2}{\pi}} i^l \equiv \Phi_{l's'ls}^{J(\pm)}(q, k, r) - \sqrt{\frac{2}{\pi}} i^l j_l(kr) \quad (3.11)$$

it satisfies the equation

$$\left(q^2 + \frac{d^2}{dr^2} - \frac{l'(l'+1)}{r^2} \right) \chi_{l's'ls}^{J(\pm)}(q, k, r) - \sum_{l''s''} 2\mu U_{l's'l''s''}^J(r) \chi_{l''s''ls}^{J(\pm)}(q, k, r) = r 2\mu U_{l's'ls}^J(r) j_l(kr) \quad (3.12)$$

and the off-shell element of \tilde{t} is given by this χ as

$$\tilde{t}_{l's'ls}^J(p, k; z) = \frac{1}{2\mu} \frac{2}{\pi} i^{-l'+l} \int_0^\infty dr r j_{l'}(pr) \left(q^2 + \frac{d^2}{dr^2} - \frac{l'(l'+1)}{r^2} \right) \chi_{l's'ls}^{J(+)}(q, k, r) . \quad (3.13)$$

Following further Ref. [20] one arrives at the analytic expression of the \tilde{t} element in Eq. (3.13). For a pure hard core potential with radius c , Eq. (3.12) has the solution

$$\chi_{l'l's'ls}^{J(\pm)}(q, k, r) = \delta_{l'l} \delta_{s's} \times \begin{cases} -r j_l(kr) & (r \leq c) \\ -\frac{j_l(kc)}{h_l^{(\pm)}(qc)} r h_l^{(\pm)}(qr) & (r \geq c) \end{cases} \quad (3.14)$$

Note that there is no coupling in ℓ and s , a result which can be found by generating the hard-core potential matrix U as limits of square well potentials (see Ref. [20]). Further, due to Eq. (3.14) the integration in Eq. (3.13) is limited to $r \leq c$ and carrying out it, we obtain the final expression for \tilde{t}

$$\begin{aligned} \tilde{t}_{l's'ls}^J(p, k; z) &= \delta_{l'l} \delta_{s's} \frac{1}{2\mu} \frac{2}{\pi} i^{-l'+l} \\ &\times \left[-c j_l(pc) \frac{d}{dr} r h_l^{(+)}(qr) \Big|_{r=c} \frac{j_l(kc)}{h_l^{(+)}(qc)} + \frac{d}{dr} r j_l(pr) \Big|_{r=c} c j_l(kc) \right. \\ &\left. - (q^2 - p^2) \int_0^c dr r^2 j_l(pr) j_l(kr) \right]. \end{aligned} \quad (3.15)$$

The last term on the right-hand side of this equation is shown in Ref. [20] to be

$$\int_0^c dr r^2 j_l(pr) j_l(kr) = \begin{cases} \frac{c^2}{k^2 - p^2} (k j_l(pc) j_{l+1}(kc) - p j_l(kc) j_{l+1}(pc)) & (p \neq k) \\ \frac{c^2}{2k} \left(k c (j_l^2(kc) + j_{l+1}^2(kc)) - (2l+1) j_l(kc) j_{l+1}(kc) \right) & (p = k) \end{cases} \quad (3.16)$$

Next, let us consider the second part of the two-potential formula (3.5). The state $\Psi_{q, \vec{k}}^{(+)}$ given in Eq. (3.2) satisfies another equation [19]

$$| \Psi_{q, \vec{k}}^{(+)} \rangle = | \Phi_{q, \vec{k}}^{(+)} \rangle + G_U(z) \hat{V} | \Psi_{q, \vec{k}}^{(+)} \rangle \quad (3.17)$$

with

$$G_U(z) = G_0(z) + G_0(z) U G_U(z) . \quad (3.18)$$

Hence, if we define \hat{t} by

$$\langle \vec{p} | \hat{t}(z) | \vec{k} \rangle \equiv \langle \Phi_{q, \vec{p}}^{(-)} | \hat{V} | \Psi_{q, \vec{k}}^{(+)} \rangle \quad (3.19)$$

then the second part of the two-potential formula becomes

$$\langle \vec{p} | \hat{t}(z) | \vec{k} \rangle = \langle \Phi_{q, \vec{p}}^{(-)} | \hat{V} | \Phi_{q, \vec{k}}^{(+)} \rangle + \langle \Phi_{q, \vec{p}}^{(-)} | \hat{V} G_U(z) \hat{V} | \Psi_{q, \vec{k}}^{(+)} \rangle \quad (3.20)$$

Observing

$$\begin{aligned} \langle \vec{p}' | G_U &= \langle \vec{p}' | G_0 (1 + U G_U) \\ &= \frac{1}{z - \frac{p'^2}{2\mu}} \langle \Phi_{q, \vec{p}'}^{(-)} | \end{aligned} \quad (3.21)$$

and applying it to the second term of the right-hand side of Eq. (3.20), we arrive at the integral equation for \hat{t}

$$\langle \vec{p} | \hat{t}(z) | \vec{k} \rangle = \langle \Phi_{q, \vec{p}}^{(-)} | \hat{V} | \Phi_{q, \vec{k}}^{(+)} \rangle + \int d\vec{p}' \langle \Phi_{q, \vec{p}}^{(-)} | \hat{V} | \vec{p}' \rangle \frac{1}{z - \frac{p'^2}{2\mu}} \langle \vec{p}' | \hat{t}(z) | \vec{k} \rangle . \quad (3.22)$$

The inputs to this integral equation, $\langle \Phi_{q, \vec{p}}^{(-)} | \hat{V} | \Phi_{q, \vec{k}}^{(+)} \rangle$ and $\langle \Phi_{q, \vec{p}}^{(-)} | \hat{V} | \vec{p}' \rangle$, are expressed by the scattering states from the pure hard-core part, $\Phi^{(\pm)}$, and the rest of the potential, \hat{V} . According to Eqs. (3.11) and (3.14), the scattering states $\Phi^{(\pm)}$ are expressed simply by spherical Bessel and Hankel functions as

$$\Phi_{l's'l's}^{J(\pm)}(q, k, r) = \begin{cases} 0 & (r < c) \\ \delta_{l'l} \delta_{s's} \sqrt{\frac{2}{\pi}} i^l \left(j_l(kr) - \frac{j_l(kc)}{h_l^{(\pm)}(qc)} h_l^{(\pm)}(qr) \right) & (r > c) \end{cases} \quad (3.23)$$

which allows one to easily calculate these inputs. Thus the integral equation (3.23) can be solved in a similar manner as described in Sec. II.

Consequently, combining the analytic expression of the first part, Eqs. (3.15) and (3.16) with the solution of this integral equation, we easily obtain the off-shell t -matrix for a hard-core potential.

IV. CUSPS AND ROUND PEAKS CAUSED BY NEARBY POLES

As we described in Sec. I, this paper mainly aims to search t -matrix poles for various YN interactions around the ΣN threshold. In Eq. (2.4), the t -matrix elements are defined by the relative momenta between the hyperons and the nucleon, q_1 in case Λ -N and q_2 in case of Σ -N. However, these momenta are not independent and are related to the energy E via Eq. (2.5). This can be rewritten as

$$\frac{q_1^2}{2\mu_1} + m_N + m_\Lambda = \frac{q_2^2}{2\mu_2} + m_N + m_\Sigma = E . \quad (4.1)$$

Thus each t -matrix element is a function of the energy E , and has branch points at the two thresholds $E = m_N + m_\Lambda$ and $E = m_N + m_\Sigma$. We therefore encounter a somewhat complicated Riemann energy surface with four sheets, and have to specify how they are related to the upper and lower halves of the q_1 and q_2 planes [15,16]. In two-channel problems, a procedure called uniformization [17] is very convenient to map the 4 Riemann sheets into one plane. This we shall use in the present analysis. This uniformization introduces another variable in place of the energy, in terms of which the t -matrix becomes single-valued. Let us introduce such a variable ω following Ref. [17]. It satisfies

$$\frac{q_1}{\sqrt{2\mu_1}} + \frac{q_2}{\sqrt{2\mu_2}} = \Delta \omega \quad (4.2)$$

$$\frac{q_1}{\sqrt{2\mu_1}} - \frac{q_2}{\sqrt{2\mu_2}} = \Delta \omega^{-1}$$

with

$$\Delta^2 \equiv m_\Sigma - m_\Lambda . \quad (4.3)$$

Apparently by that ansatz (4.2) one fulfills (4.1). These equations constitute a mapping of the Riemann energy surface to the complex ω plane which is shown in Fig. 1. There are, of course, 4 possible quadrants where q_1 is located, and for each q_1 two different values of q_2 are allowed by Eq. (4.1). Hence we have 8 possible cases in specifying to which quadrants both q_1 and q_2 belong on their own complex planes. The complex ω plane in Fig. 1 is divided accordingly into 8 parts, in each of which the two numbers inside the square brackets indicate the quadrants to which q_1 and q_2 belong. The bold line expresses the region where bound or scattering states exist if present. The ΛN threshold is located at $\omega = i$, while the ΣN threshold resides at $\omega = 1$. If one moves counter-clockwise around $\omega = i$, the quadrant to which q_1 belongs changes as $1 \rightarrow 2 \rightarrow 3 \rightarrow 4$ (the first numbers inside the square brackets), and at the same time the quadrant of q_2 changes as $1 \rightarrow 2 \rightarrow 1 \rightarrow 2$ (the second numbers inside the square brackets). On the other hand, if one moves around $\omega = 1$ which corresponds to the ΣN threshold, the quadrant to which q_2 belongs varies as $1 \rightarrow 2 \rightarrow 3 \rightarrow 4$ and the quadrants of q_1 as $1 \rightarrow 4 \rightarrow 1 \rightarrow 4$.

Let us now consider the relation between the shapes of the ΛN elastic total cross section and the positions of a pole near the ΣN threshold. The big difference to single channel problems is that there exists the region [1,3] touching the ΣN threshold. (Here we use the square bracket with the same meaning as in Fig. 1.) Suppose a pole exists in this region close to the threshold, then the ΛN elastic total cross section takes the shape of a cusp just at the threshold. On the other hand, if a pole resides in the region [4,2] or [4,4] close to the bold line in Fig. 1, the cross section shows a round peak of the Breit-Wigner form. A pole lying in [4,2] is often called an unstable bound state(UBS) pole [7]. We shall now discuss the above mentioned behavior of the cross sections. Let us assume the t -matrix has a pole at the position $(q_1, q_2) = (\alpha_1, \alpha_2)$, and the corresponding energy is E_0 . It follows

$$E_0 = \frac{\alpha_1^2}{2\mu_1} + m_N + m_\Lambda = \frac{\alpha_2^2}{2\mu_2} + m_N + m_\Sigma . \quad (4.4)$$

Then, around the pole the t -matrix elements can be approximated as

$$\langle p | T_{ij}(E) | p' \rangle \simeq \frac{R_{ij}(p, p')}{E - E_0} \quad (4.5)$$

The approximation (4.5) of a first-order pole holds even in the case that it resides in Riemann sheets other than the first one, which is proved for example in Ref. [21] for a single channel case. The extension to the coupled $\Lambda N - \Sigma N$ system is straightforward. Notice however for all the pairs of $(q_1, q_2) = (\pm\alpha_1, \pm\alpha_2)$ the energies defined by Eq. (4.1) take the same value E_0 but reside in different places on the Riemann energy surface. The approximation (4.5) is valid only around $(q_1, q_2) = (\alpha_1, \alpha_2)$.

Now, according to Eqs. (4.1) and (4.4), we rewrite Eq. (4.5) as

$$\langle p | T_{ij}(E) | p' \rangle \simeq \frac{\tilde{R}_{ij}(p, p')}{q_1 - \alpha_1} \quad (4.6)$$

or

$$\langle p | T_{ij}(E) | p' \rangle \simeq \frac{\bar{R}_{ij}(p, p')}{q_2 - \alpha_2} . \quad (4.7)$$

However, the expression (4.6) is not appropriate around the ΣN threshold. As already mentioned this is because if one moves the pole around the ΣN threshold, the quadrant to which α_1 belongs changes as $1 \rightarrow 4 \rightarrow 1 \rightarrow 4$, while the quadrant in which α_2 is located changes as $1 \rightarrow 2 \rightarrow 3 \rightarrow 4$. The expression (4.6) therefore can not distinguish whether the pole sits in the regions [4,2] or [4,4], or in the regions [1,1] or [1,3]. This is not the case with the expression (4.7), which we shall use. Let us now infer from Eq. (4.7) shapes of the ΛN elastic total cross section σ around the ΣN threshold. Since

$$\sigma \propto | \langle q_1 | T_{11}(E) | q_1 \rangle |^2 \quad (4.8)$$

the q_2 dependence of the cross section becomes roughly

$$\sigma \propto \left| \frac{1}{q_2 - \alpha_2} \right|^2 \quad (4.9)$$

Writing $\alpha_2 = a + ib$, we have

$$\sigma \propto \begin{cases} \frac{1}{(|q_2| - b)^2 + a^2} & (q_2 = i|q_2| : \text{below the } \Sigma N \text{ threshold}) \\ \frac{1}{(q_2 - a)^2 + b^2} & (q_2 > 0 : \text{above the } \Sigma N \text{ threshold}) \end{cases} \quad (4.10)$$

For the three cases, that the pole is located in the regions [4,2], [1,3] and [4,4], we plot the cross sections σ expressed by Eq. (4.10) in Figs. 2, 3 and 4, respectively. Notice that Figs. 2(c), 3(c) and 4(c) show the cross section as a function of the energy E , hence its derivative at the threshold energy is infinite according to the relation (4.1). If the pole is located in the regions [4,2] or [4,4] (Figs. 2(c) or 4(c)), the cross sections show round peaks of the Breit-Wigner form. They are quite similar to the resonances in single channel problems. In contrast, if the pole sits in the region [1,3], the cross section forms a big cusp just at the threshold (Fig. 3(c)). In Ref. [16], this type of poles are named inelastic virtual state poles. We should recognize that such a big cusp is caused by the pole, and is not a simple threshold effect. Some of such poles, as we shall show in the next section, actually move into the region [4,2] and convert to unstable bound state (UBS) poles when the potential strength is slightly increased.

V. RESULTS

We searched t -matrix poles for various meson theoretical YN interactions in the manner described in Secs. II and III. We use the soft core model (NSC89) [5] and the hard core models D [12] and F [13] (abbreviated as ND and NF respectively) of the Nijmegen group. This group has recently proposed a new soft core model (NSC97) [14], which includes six different versions named a, b, c, d, e and f. Among them we analyze NSC97f. Both soft core models NSC89 and NSC97f we use reproduce the correct binding energy of the hypertriton [2,3,22]. The hard-core potentials were also chosen because they are still used in hypernuclear physics studies.

Before proceeding to the positions of poles, we show in Fig. 5 the ΛN elastic total cross sections around the ΣN threshold for these force models. The model NF yields a round peak, while ND and NSC89 form the cusps just at the threshold. For NSC97f, the shape is not definite. We find all the enhancements are caused by the ${}^3S_1 - {}^3D_1$ force component. With regard to experimental situations, there exist only sparse data of the ΛN cross sections, which can not determine the actual shape. However a prominent peak around the ΣN threshold was observed in the $K^- + d \rightarrow p + \Lambda + \pi^-$ reaction [23].

For every potential we use, we found a pole near the ΣN threshold in the $^3S_1 - ^3D_1$ wave. They are shown in Table I. In Fig. 6, the poles are also displayed in the complex q_2 ($\Sigma - N$ relative momentum) plane. For NSC97f and NF, the poles are located in the [4,2] region of the ω plane, while for NSC89 and ND, they lie in the region [1,3]. The relation between the position of a pole and the shape of the $\Lambda - N$ cross section described in Sec. IV holds here for all potentials except for NSC97f. The pole for NSC97f is close to the boundary between the regions [4,2] and [1,3], and it is farther from the imaginary axis of the q_2 plane than for NF, which explains why the shape of the ΛN cross sections for this potential is not a clear-cut example of a cusp or a round peak type. Thus this pole lies in a gray area between the regions [4,2] and [1,3]. Anyway, for all the interaction models the poles are close to the ΣN threshold and cause some enhancements. For NSC97f, the unstable bound state exists in the two-body YN system, and very likely in the YNN system. As for the locations of poles in the complex energy sheets, we refer the readers to [16] where those are nicely illustrated. We also emphasize that one should not consider the poles in the region [1,3] which produce the cusps as less important. We actually calculated a trajectory of the pole for the potential ND, multiplying it by an overall strength parameter λ . The trajectory is shown in Fig 7. The pole moves from the region [1,3] into [4,2] as the potential strength increases, and becomes an unstable bound state pole.

Now we regard the fact that poles also exist near the ΛN threshold. In Table II, the antibound-state poles below this threshold are shown for the 1S_0 and $^3S_1 - ^3D_1$ waves. The 1S_0 poles are relatively close to the threshold, and correlated to the scattering length, as one expects. The ΛN scattering lengths, as we mentioned, are not yet determined because of scant cross section data. However, the analyses of the hypertriton [2,3,22] constrain the S -wave scattering lengths. The potentials NSC97f and NSC89 which reproduce both of the hypertriton binding energy and the ΛN cross section data have the 1S_0 scattering length within -2.6 to -2.4 fm, and the 3S_1 scattering length within -1.7 to -1.3 fm. The corresponding position of the 1S_0 pole is at about $-0.27i$ fm $^{-1}$ in the $q_1(\Lambda - N$ relative momentum) complex plane.

Finally, we would like to point out that the analyses of the kaon photoproduction processes, $d(\gamma, K^+)YN$ or $^3\text{He}(\gamma, K^+)YNN$ are very promising to clarify the effects caused by the YN final-state interaction around the ΛN and ΣN thresholds. Experimentally those reactions are feasible at TJLAB and SPring-8. Further and importantly for the theoretical description, the interactions of the photon and of the K^+ meson with the baryons are comparatively weak, which enables one to formulate and calculate these reactions rather well. All the techniques and the insights gained in this article are immediately applicable to those reactions and we plan to perform such calculations.

ACKNOWLEDGMENTS

We would like to thank W.Glöckle for the careful reading of the manuscript and for critical and helpful comments.

REFERENCES

- [1] K. Miyagawa and W. Glöckle, Phys. Rev. **C48**, 2576 (1993).
- [2] K. Miyagawa, H. Kamada, W. Glöckle, and V. Stoks, Phys. Rev. **C51**, 2905 (1995).
- [3] W. Glöckle, K. Miyagawa, H. Kamada, J. Golak and H. Witała, Nucl. Phys. **A639**, 297c (1998).
- [4] E. Hiyama, M. Kamimura, T. Motoba, T. Yamada and Y. Yamamoto, Nucl. Phys. **A639**, 169c (1998).
- [5] P.M.M. Maessen, Th.A. Rijken, and J.J. de Swart, Phys. Rev. **C40**, 2226 (1989).
- [6] A. Reuber, K. Holinde, and J. Speth, Czech. J. Phys. **42**, 1115 (1992); Nucl. Phys. **A570**, 543 (1994).
- [7] See Ref. [16], and the references are therein.
- [8] T. Nagae, *Proceedings of the 25th INS International Symposium on Nuclear and Particle Physics with High-Intensity Proton Accelerators*, edited by T.K. Komatsubara, T. Shibata and T. Nomura (World Scientific, Singapore, 1997), p.265.
- [9] T. Harada, S. Shinmura, Y. Akaishi, and H. Tanaka, Nucl. Phys. **A507**, 715 (1990); T. Harada, Nucl. Phys. **A547**, 165c (1992).
- [10] I.R. Afnan and B.F. Gibson Phys. Rev. **C47**, 1000 (1993).
- [11] J. Reinhold *et al.* Nucl. Phys. **A639**, 197c (1998).
- [12] M.M. Nagels, T.A. Rijken, and J.J. de Swart, Phys. Rev. **D15**, 2547 (1977).
- [13] M.M. Nagels, T.A. Rijken, and J.J. de Swart, Phys. Rev. **D20**, 1633 (1979).
- [14] Th.A. Rijken, V.G.J. Stoks, and Y. Yamamoto, Phys. Rev. **C59**, 21 (1999).
- [15] B.C. Pearce and B.F. Gibson Phys. Rev. **C40**, 902 (1989).

- [16] A.M. Badalyan, L.P.KoK, M.I.Polikarpov, and Yu.A. Simonov, Phys. Rep. **82**, 31 (1982).
- [17] R.G. Newton, *Scattering Theory of Waves and Particles* (McGraw-Hill, New York, 1966)
- [18] W. Glöckle, *The Quantum Mechanical Few-Body Problem* (Springer-Verlag, Berlin, 1983).
- [19] M.L. Goldberger and K.M. Watson, *Collision Theory* (Wiley, New York, 1964)
- [20] T. Takemiya, Prog.Theor. Phys. **48**, 1547 (1972); **49**, 1602 (1973).
- [21] Ch. Elster, J.H. Thomas, and W. Glöckle, Few-Body Systems **24**, 55 (1998).
- [22] K. Miyagawa (private communication).
- [23] R.H. Dalitz and A. Deloff, Czech. J. Phys. **B32**, 1021 (1982) and the references are therein.

TABLES

TABLE I. The poles near the ΣN threshold for the component $^3S_1 - ^3D_1$ of the various force models. The positions of the poles are shown on the complex planes of the relative momenta in the ΛN and ΣN channels, q_1 and q_2 , respectively. The corresponding center-of-mass energies are indicated by E .

model	q_1 (fm $^{-1}$)	q_2 (fm $^{-1}$)	E (MeV)
NSC97f	(1.46, -0.04)	(-0.35, 0.15)	(2135.6, -3.89)
NSC89	(1.37, 0.01)	(-0.04, -0.39)	(2126.3, 1.07)
ND	(1.43, 0.01)	(-0.18, -0.08)	(2132.8, 1.07)
NF	(1.44, -0.02)	(-0.28, 0.12)	(2134.2, -2.49)

TABLE II. The poles below the ΛN threshold. The scattering lengths indicated by a are also shown. See the caption to Table I for other details.

model	partial wave	q_1 (fm $^{-1}$)	q_2 (fm $^{-1}$)	E (MeV)	a (fm)
NSC97f	1S_0	(0, -0.27)	(0, 1.47)	(2051.8, 0)	-2.59
	$^3S_1 - ^3D_1$	(0, -0.37)	(0, 1.49)	(2049.3, 0)	-1.70
NSC89	1S_0	(0, -0.28)	(0, 1.47)	(2051.5, 0)	-2.48
	$^3S_1 - ^3D_1$	(0, -0.45)	(0, 1.51)	(2046.8, 0)	-1.32
ND	1S_0	(0, -0.35)	(0, 1.49)	(2050.0, 0)	-1.83
	$^3S_1 - ^3D_1$	(0, -0.35)	(0, 1.49)	(2050.0, 0)	-1.89
NF	1S_0	(0, -0.31)	(0, 1.48)	(2050.8, 0)	-2.19
	$^3S_1 - ^3D_1$	(0, -0.36)	(0, 1.49)	(2049.7, 0)	-1.83

FIGURES

FIG. 1. The complex ω plane into which the energy Riemann surface is mapped. The two numbers inside the square brackets indicate the quadrants to which q_1 and q_2 belong respectively. (The relation between the energy E and the momenta q_1 and q_2 is given by Eq. (4.1).) The parentheses show whether q_1 and q_2 are positive, negative, positive imaginary, or negative imaginary, respectively. The bold line expresses the region where bound or scattering states exist if present.

FIG. 2. The shape of the ΛN elastic total cross section σ around the ΣN threshold in the case a nearby t -matrix pole is located in the region [4,2]. (The pole resides the 2nd quadrant of q_2 .) The cross sections σ given by Eq. (4.10) are plotted, (a) as a function of $|q_2|$ below the threshold, (b) as a function of q_2 above the threshold, and (c) as a function of E .

FIG. 3. Same as Fig. 2 but for the case a t -matrix pole is located in the region [1,3]. (The pole resides the 3rd quadrant of q_2 .)

FIG. 4. Same as Fig. 2 but for the case a t -matrix pole is located in the region [2,4]. (The pole resides the 4th quadrant of q_2 .)

FIG. 5. The ΛN elastic total cross sections around the ΣN threshold as a function of Λ lab momentum. The predictions by the force models of the Nijmegen group NSC97f, NSC89, ND and NF are shown.

FIG. 6. The positions of the poles for the force models NSC97f, NSC89, ND and NF in the complex q_2 plane.

FIG. 7. The trajectory of the pole for the potential ND in the complex q_2 plane with the multiplied overall strength parameter λ .

Fig. 1

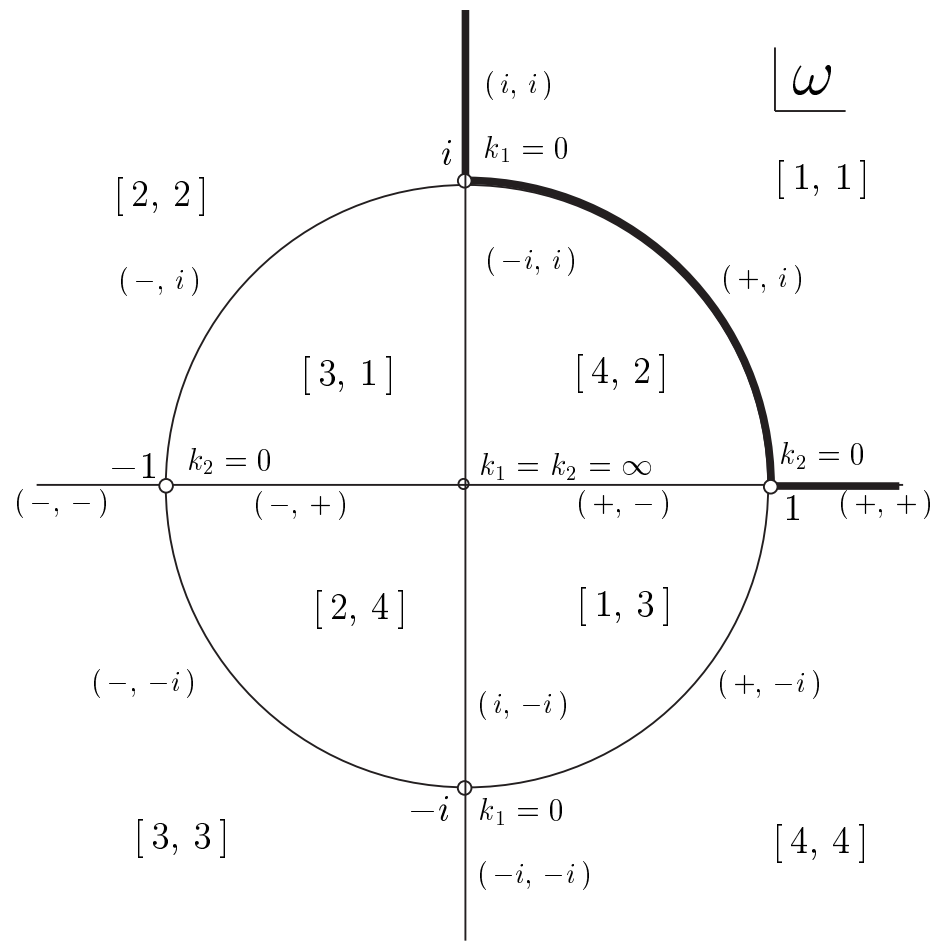


Fig. 2

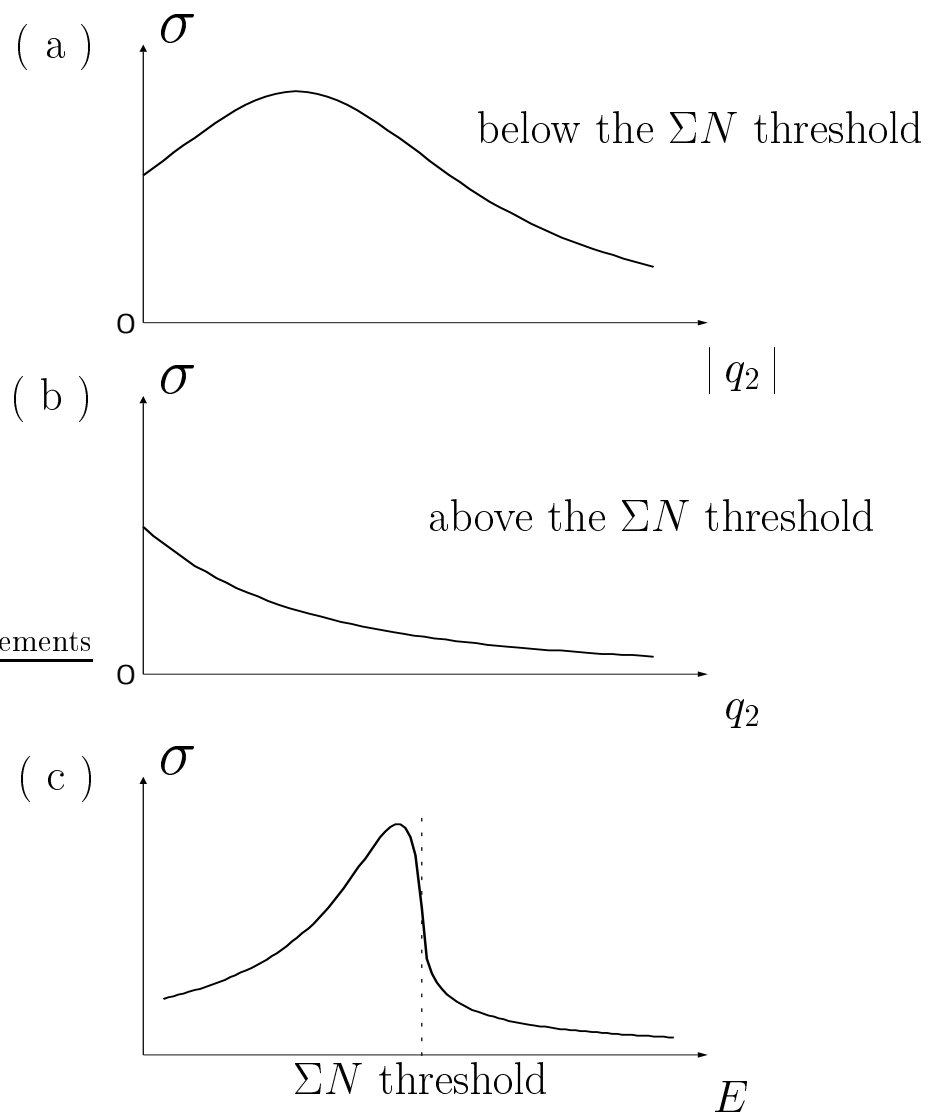


Fig. 3

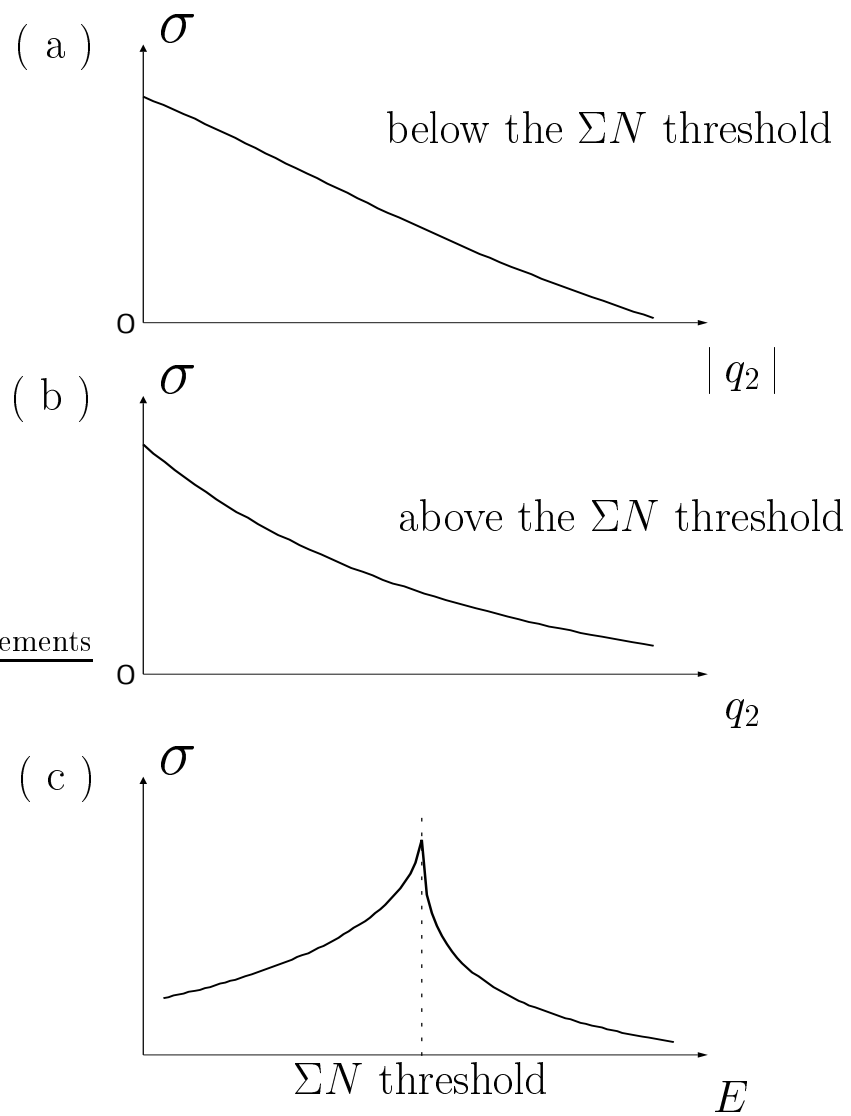


Fig. 4

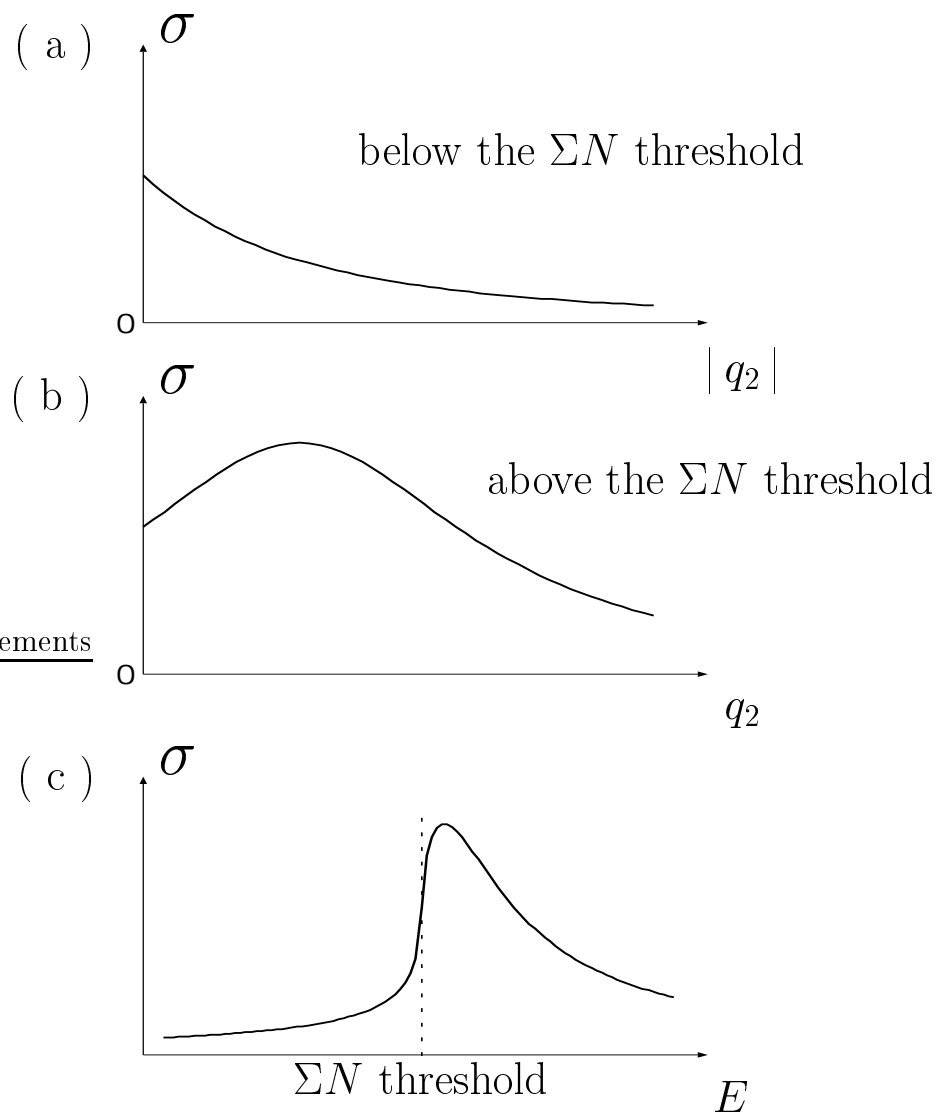


Fig. 5

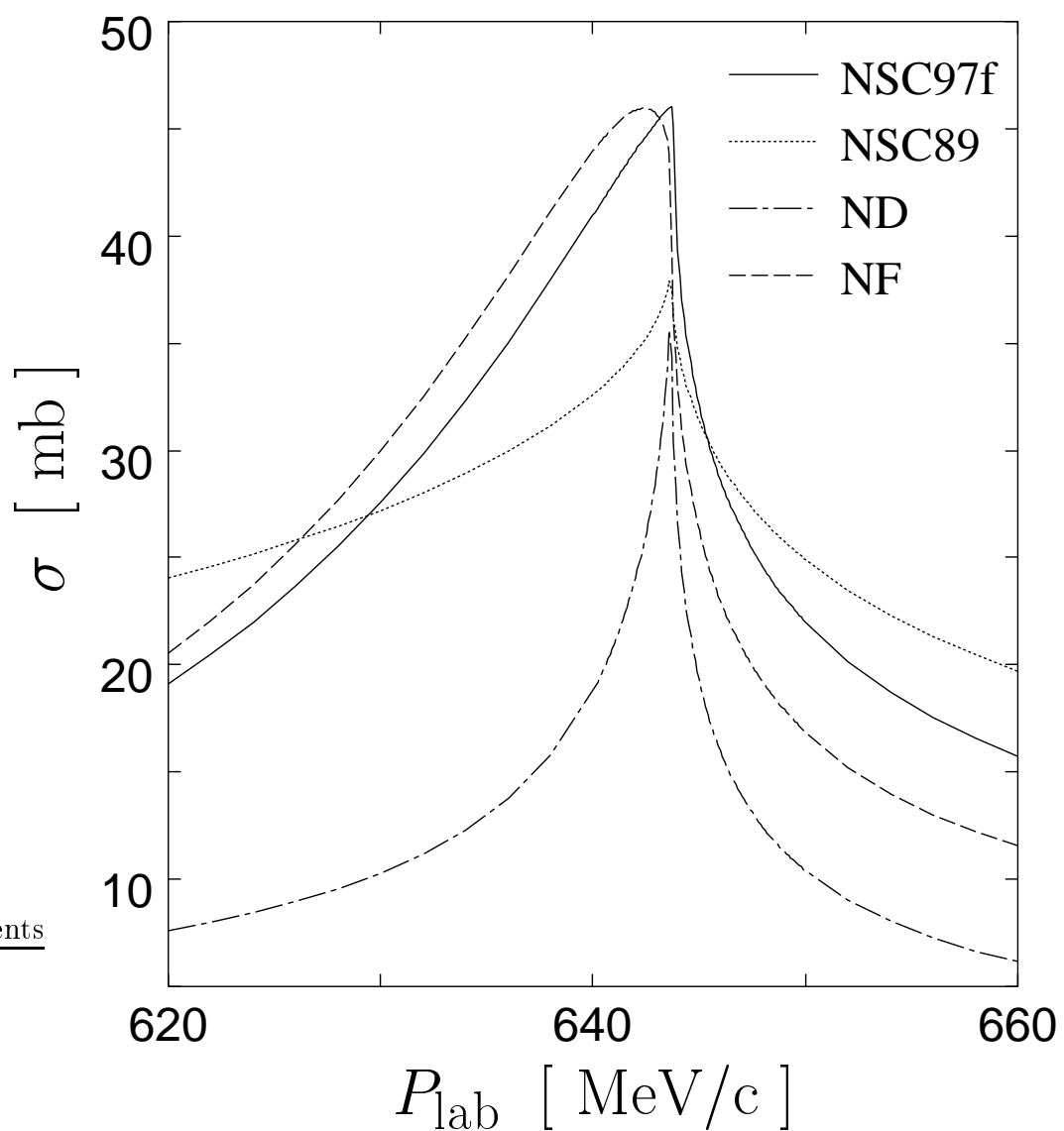


Fig. 6

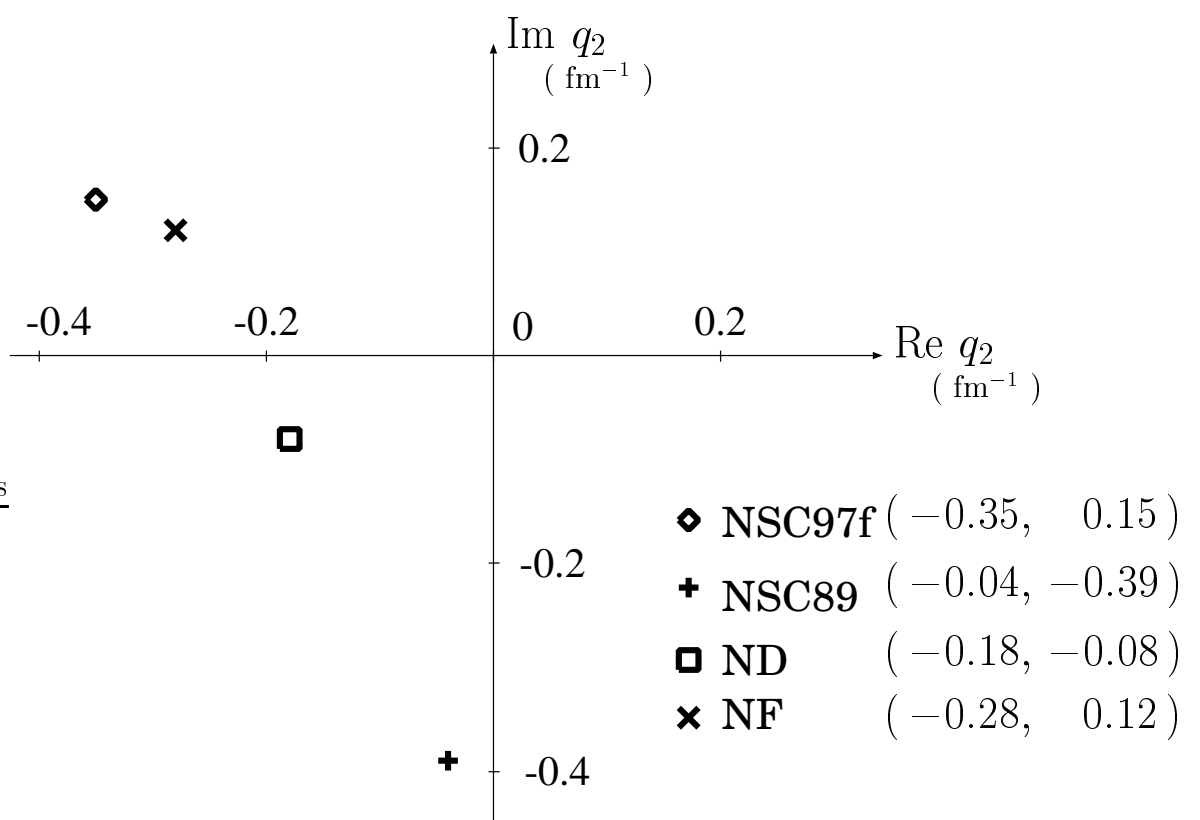


Fig. 7

